Toward precision biomarker RAI therapy of well-differentiated thyroid cancer: linking administered radioactivity (MBq) to a prescribed lesion radiation-absorbed dose (cGy)

Audrey Mauguen
Memorial Sloan Kettering Cancer Center
Ravinder Grewal
Memorial Sloan Kettering Cancer Center
Finn Augensen
Memorial Sloan Kettering Cancer Center
Murad Abusamra
Memorial Sloan Kettering Cancer Center
Sonia Mahajan
New York University Grossman School of Medicine
Vetri Sudar Jayaprakasam
Memorial Sloan Kettering Cancer Center
Joseph Osborne
Weill Cornell Medical College: Weill Cornell Medicine
Keith Pentlow
Memorial Sloan Kettering Cancer Center
Sofia Haque
Memorial Sloan Kettering Cancer Center
James Fagin
Memorial Sloan Kettering Cancer Center
Heiko Schoder
Memorial Sloan Kettering Cancer Center
Michael Tuttle
Memorial Sloan Kettering Cancer Center
Alan Ho
Memorial Sloan Kettering Cancer Center
John Humm
Memorial Sloan Kettering Cancer Center
Steven Larson (larsons@mskcc.org)
Memorial Sloan Kettering Cancer Center https://orcid.org/0000-0002-6111-7507

Research Article

Keywords: Differentiated thyroid cancer, dosimetry, Iodine-124, PET/CT, radioactive iodine therapy

Posted Date: October 24th, 2022

DOI: https://doi.org/10.21203/rs.3.rs-2156223/v1

Version of Record: A version of this preprint was published at European Journal of Nuclear Medicine and Molecular Imaging on May 12th, 2023.
See the published version at https://doi.org/10.1007/s00259-023-06240-1.

Abstract

Purpose

To introduce a biomarker-based dosimetry method for radioactive iodine ^{131}I therapy (RAI) of metastatic differentiated thyroid cancer (mDTC), adapted to the underlying heterogeneity of lesions' radiation-absorbed dose (RAD) in cGy, and permitting 1) estimates of RAD/lesion with known precision and 2) optimization of patient-specific administered amount of radioactive iodine (^{131}I) in MBq.

Methods

Patients referred for RAI therapy of mDTC were enrolled in institutionally approved protocols. A total of 208 mDTC lesions (in 21 patients) with SUV > 1 underwent quantitative PET scans at 24, 48, 72, and 120 hours post-administration of 222 MBq of theranostic NaI-^{124}I to determine the individual lesion RAD (in cGy) based on MIRD 2020 guidance. Using a general estimating equation, a prediction curve for biomarker development was generated in the form of a best-fit regression line and 95% prediction interval, correlating individual predicted lesion RAD metrics, with candidate biomarkers ("predictors") such as SUV and activity in microcurie per gram, from a single imaging timepoint.

Results

In the 169 lesions (in 15 patients) that received ^{131}I therapy, individual lesion cGy varied over 3 logs with a median of 22,000 cGy, confirming that heterogeneity of lesion RAD was profound. Initial findings from the prediction curve on all 208 lesions confirmed that 48h SUV was the best predictor of lesion RAD and permitted calculation of the ^{131}I required (in MBq) to achieve a lesional threshold dose for response (2,000 cGy) in more than 95% of lesions.

Conclusions

Based on MIRD lesion RAD estimates and regression statistics, we propose and report initial feasibility for an ^{124}I-PET-based dosimetry biomarker for RAI in patients with mDTC. This approach enables clinicians to select personalized (precision) therapeutic administration of radioactivity (MBq) to achieve a desired target lesion-absorbed doses (cGy) for > 95% of all lesions using a single 48-hour measurement ^{124}I-PET image.

NCT04462471, Registered July 8, 2020.

NCT03647358, Registered Aug 27, 2018.

Introduction

Precision medicine strives to tailor the best possible treatment to the unique cancer of an individual patient. Distant metastases are detected in 3–20% of patients with differentiated thyroid cancer (DTC) at some point in the course of their disease (*1*). For advanced thyroid cancer, treatment of metastatic DTC (mDTC) with radioiodine ^{131}I therapy (RAI) has been lifesaving for many patients (*2*). However, not all patients benefit, and side effects can be significant. It is known that response of thyroid cancer to RAI is radiation dose-related, but unlike modern external beam radiotherapy, there are no widely accepted dosimetry methods to predict which patients with metastatic thyroid cancer are likely to respond to RAI therapy. Accordingly, many patients continue to receive multiple empirical therapeutic doses of ^{131}I that may be ineffective and can cause considerable morbidity, with potential toxicity to the bone marrow, lung, and salivary glands.

Several investigators have proposed the use of ^{124}I as a theranostic solution to the problem of RAI dosimetry (*3–5*). Iodine-124 is a 4.2-day half-life positron-emitting isotope that allows for serial PET imaging over several days, enabling accurate lesion dosimetry using the MIRD approach (MIRD 2021). A simple correction for the physical half-life and emissions between imaging isotope ^{124}I and therapeutic isotope ^{131}I provides the capability to predict the lesion doses from a planned ^{131}I therapy administration. Such radionuclide dosimetry may allow nuclear medicine physicians and referring physicians alike to better identify patients likely to benefit from RAI and those who will not, thereby preventing unnecessary treatment when the predicted tumor doses are below the levels required to achieve therapeutic responses.

A common clinical problem is that some patients are refractory to ^{131}I RAI (RAIR); this resistance is most often because their tumors do not concentrate and retain sufficient RAI to be tumoricidal. Our interest in ^{124}I was intensified based on the discoveries of Fagin et al (*6*), who demonstrated that kinase inhibitors of the MAP-kinase pathway, particularly MEK and BRAF inhibitors, could reinduce RAI tumor uptake in laboratory models of BRAF-mutant thyroid cancer (*7*). Accordingly, we investigated the potential of a single-timepoint dosimetry method using PET/CT ^{124}I imaging, based on what we called the 48/48-hour rule (48-hour timepoint, 48-hour effective half-life). In a group of patients with RAIR

thyroid cancer studied by Ho et al (*8*), we found that single-timepoint quantitative PET imaging at 48 hours could successfully be used to select patients for RAI therapy. An increase in radioiodine uptake induced by a four-week course of a kinase inhibitor (determined by ^{124}I-uptake with PET imaging performed at 48 hrs) that predicted a radiation-absorbed dose greater than 2,000 centiGray (cGy) correlated with a partial response 6 months post-RAI per RECIST criteria in 5/8 patients (*7*).

In the present study, we introduce a regression-based RAI dosimetry tool for mDTC with a known precision that builds on these earlier findings in the RAIR setting. Our hypothesis was that a practical and clinically useful dosimetry biomarker could be developed using single-timepoint ^{124}I PET imaging, to 1) reliably predict ^{131}I RAI lesion radiation-absorbed dose for all active lesions in an individual patient; and 2) optimize selection of administered activity (MBq) necessary to achieve at least the minimum radiation dose needed to reliably induce a treatment effect. If successful, this approach could offer practical guidance for selecting treatment activities for patients with heterogeneous radioiodine uptake that would produce lesion doses within an expected statistical prediction interval. Secondly, we anticipate a possible refined and more widespread application of the methodology for advanced research with application to novel targeted therapies used to enhance the effectiveness of RAI.

In this manuscript, we discuss the workflow based on serial quantitative ^{124}I PET imaging with dosimetry estimates derived from the lesion uptake and clearance kinetics of individual lesions. Our approach sought to determine the best single-timepoint imaging and test its precision as a predictor of lesion dosimetry, minimizing the need for four-timepoint data acquisition. Our main motivation and rationale for developing the ^{124}I PET imaging biomarker approach was to devise a practical and simple methodology for determination of lesional dosimetry that would be combined with standard blood and whole-body clearance dosimetry to optimize ^{131}I RAI recommendations for patients with mDTC.

Methods

Population

This study includes lesions from consecutive patients studied at MSK under two different IRB-approved protocols,18–253 and 20–053, who underwent imaging between March 2019 and August 2021. Patients who were considered candidates for RAI treatment of DTC were enrolled after giving informed consent. All patients had histologically confirmed metastatic thyroid cancer (Table 1).

Individualized Lesion Kinetics and Dosimetry

Lesions were scanned at four timepoints by PET/CT after oral administration of a diagnostic activity 222 MBq (6.0 mCi) of ^{124}I-NaI (3D Imaging, Waco, TX). Whole-body imaging was performed on a GE D710 PET/CT scanner at the nominal times: 24, 48, 72, and 96 hours post-administration (Fig. 1). ^{124}I PET reconstructions were performed in a 128*128 matrix, 2 iteration, 16 subsets, with in-plane smoothing with a 6.4 mm FWHM Gaussian kernel and GE z-axis heavy smoothing with the prompt gamma correction turned on. Regions of interest (ROI) were placed over all visible lesions > 0.5 cm within the body using ^{124}I PET/CT and the diagnostic CT images. From each ROI, the following parameters were recorded in an Excel database for each patient and each lesion: size in three dimensions (cm); standardized uptake value (SUV) by weight and by lean body weight, both maximum and average; and activity concentration in MBq/gram or microcurie/gram (Table 2). For these patients, we estimated the best clearance fitting curve using a three-parameter (a_0, λ_1 and λ_2) dual exponential equation model comprising lesion uptake $a_0(1-\exp^{-(\lambda_1 t)})$ and clearance ($\exp^{-(\lambda_2 t)}$). Prior to integration, clearance fitting was adjusted to replace the decay constant of ^{124}I with ^{131}I, used for therapy. This AUC was multiplied by the equilibrium dose constant (10.95 g.cGy/MBq.hr or 0.405g.cGy/μCi.hr) for the non-penetrating β-emissions of ^{131}I to yield the lesion-absorbed dose in cGy.

Predicting AUC Based on a Single Timepoint

A goal of this study is to develop a statistical model to predict the calculated lesion dosimetry derived from four-timepoint imaging with fitted radioiodine kinetics from a single image acquisition timepoint. If successful, this would obviate the need for costly additional PET/CT imaging needed to fully characterize the kinetic behavior. The approach starts with estimating the linear relationship between the full dosimetry derived from the AUC from fitting four measured timepoints and the activity measured at one timepoint, called the predictor (e.g., SUV at 48h; see Fig. 2). The AUC for an individual lesion is directly proportional to the absorbed dose by a multiplicative factor, the equilibrium dose constant, which describes the emission properties of the radionuclide. For this estimation, the unit is the lesion, and a generalized estimating equation approach is used to estimate the parameters (intercept, slope, and robust variance matrix) accounting for the correlation between lesions in the same patient. Log-transformed values of the uptake and doses are used to ensure the data are normally distributed. The linear model is as follows, where the errors ϵ_{ij} are correlated, y_{ij} is the logarithm of the AUC value, and x_{ij} is the uptake measured at one timepoint; e.g., the logarithm of 48h SUV measured for the lesion *j* from patient *i*:

$$y_{ij} = x\prime_{ij}\beta + \epsilon_{ij}$$

Second, using the estimations for β and the covariance matrix, a prediction interval (PI) is calculated. A PI differs from a confidence interval, as it aims to predict with 95% confidence where future measurements will fall. In our case, if we observed the same value of SUV at 48h for 100 new

lesions, the PI is the range in which 95 of those lesions' AUCs will be found. As difficulties arose when analytically constructing the PI, we used simulated prediction to calculate PIs following the steps detailed in Gelman and Hill (2007) and summarized in Appendix A.

To validate the accuracy of the prediction, we used a leave-one-patient-out cross-validation approach. For each patient $i (i = 1, \ldots, n)$, the linear regression parameters are re-estimated using $n - 1$ patients (excluding i), and PIs are calculated for each lesion based on their measured predictor values. For those lesions, the actual observed AUC is then compared to the PI. When using 95% PI, it is expected that 95% of the observed values will fall into the corresponding PIs; i.e., 5% will be outside the prediction. In addition, for each left-out patient, an error of prediction is calculated corresponding to the squared difference between the predicted and true AUC values for each lesion. This squared error is average over all the lesions of all the patients to obtain a cross-validated error.

Range of ^{131}I Activity to Treat a Chosen Efficacy Rate for RAI in mDTC Patients

The minimum acceptable target radiation dose of 2000 cGy was chosen because doses above this level are often used as the threshold for lesions to receive further radioiodine treatment (*10*). Based on the PI available for the AUC, a simple calculation of the relationship between ^{124}I and ^{131}I uptake can yield a PI for the dose [d_{low} – d_{high}]. For a 95% PI, the interval shows the ^{131}I activity that will ensure a dose of 2000 cGy in 95% of the lesions with the corresponding measured uptake. Thus, the higher boundary (d_{high}) corresponds to the activity to treat 97.5% of the lesions with the given uptake. By varying this boundary, it is possible to select an activity that will target 95%, 90%, or fewer of the lesions. This provides the treating physician with information necessary to select a balance between the activity needed and the predicted efficacy.

Memorial Sloan Kettering Maximum Tolerated Activity (MTA)

Since 1962, MSK clinicians have employed a series of simple blood and whole-body clearance dosimetry benchmarks that provided guidelines for MTA (*11*). These guidelines have shown a remarkable safety record with respect to avoidance of serious toxicity to lung and bone marrow during high-dose RAI treatment for differentiated thyroid cancer. To perform these studies, serial blood samples and total body measurements are conducted to determine β- and photon radiation dose contributions to blood (a surrogate for the dose-limiting bone marrow) from a pre-therapy tracer administration of ^{131}I but which is readily adapted to ^{124}I as in this study. This MTA information provides the prescribing physician with an upper bound for the administered treatment activity of ^{131}I, which can be used in combination with statistical lesion dose predictions to select the most appropriate treatment activity for that specific patient. The patients enrolled in this study were administered activities that did not exceed the maximum safe amount based on blood and whole-body clearance fitting as described by Furhang et al (*12*).

Results

Patients

At present, we have analyzed data from 208 lesions in 21 individual patients. The median age was 57 years (range: 22–85) and 62% were male (Table 1). All had distant metastases. Patients had between 3 and 23 lesions (median = 11). From this cohort, 71% (15 patients, 169 lesions) were treated by ^{131}I, with administered activities ranging from 1.70 to 15.06 GBq (46 to 407 mCi).

Dosimetry

A full lesion dosimetric analysis based on the four ^{124}I PET imaging timepoints was performed. An example of some of the data determined for patient #1 is shown in Table 2. The full parameter dataset consists of: anatomical descriptor, mean size (cm), lesion dose per projected unit millicurie of administered ^{131}I activity with and without partial volume correction (*13*), half-life based on a linear slope between day 3 and 5 as well as based on exponential curve fitting, area under the curve based on an integrated curve fit, estimated activity per gram at 48 and 72 hours post-administration, SUV and SUL (based on lean body mass) at 24, 48, and 72 hours post-administration, the administered activity to deliver 2,000 cGy, the radiation dose estimate for the administered therapy to the patient, and the maximum projected dose that could have been achieved had the maximum tolerated activity been administered. This dataset was used as the input to derive a statistical model to predict the radiation dose to lesions. The dosimetry summary for all patients is given in Supplemental Table 1.

Prediction of Activity to Deliver 2000 cGy

The prediction is limited to lesions with an SUV > 1, as no treatment is planned for lesions with no differential uptake. Lesion-absorbed doses were also calculated for lesions that received no treatment (n = 39) and included in the analysis, to include patients with low radioiodine avidity. For the dataset analyzed, the estimated regression coefficient (slope) is 1.002 (robust se = 0.024; 95% confidence interval: 0.954 to 1.049; p < 0.0001). The full predicted value of AUC based on 48h uptake can be calculated as: $\widehat{\mathrm{AUC}} = \exp\left(0.697 + 1.002.\ln\left(\mathrm{SUV}_{48}\right)\right)$.

Figure 2 illustrates each lesion according to its ln-SUV_{48} value as measured, and the ln-AUC as measured based on the four timepoints. As expected, a few data points fall outside the PI, but the PI covers the majority of lesions. To assess whether this prediction is accurate for lesions from new patients, the leave-one-out cross-validation was done for all 21 patients (Fig. 3). In all but 12 of the 208 lesions (6%, from 7/21

patients), the actual AUC based on four timepoints fell into the 95% PI. Based on the 48h timepoint, our model shows good performance and demonstrates feasibility of using one timepoint to guide treatment decisions. Table 4 shows the predicted required activities for a plausible range of lesion uptakes. Using the activity led to higher prediction error, while the use of SUL led to very similar prediction errors to those of SUV (Table 4). In addition, the prediction from other timepoints was reasonable but not as good as the 48h timepoint, with CV prediction error for SUV of 0.472 at 24h and 0.327 at 72h versus 0.223 for 48h SUV.

Subset Selected for High-dose RAI Therapy

Patients were chosen for RAI when known lesions showed active uptake of radiotracer predicted to be > 2000 cGy with the selected administered activity for each individual patient based on the MTA and other clinical parameters by a multidisciplinary tumor board. A subset of 15/21 patients representing 169/208 lesions subsequently underwent RAI therapy. The median lesion dose based on AUC was 22,305 cGy (interquartile range: 8,551 – 52,921, range: 163–906,218 cGy; Fig. 4). Assuming a linear relationship between the lesion uptake profiles measured by ^{124}I PET dosimetry and the ^{131}I therapy administered to patients, we determined that of the 169 treated lesions, 163 (96%) received a dose greater than 2000 cGy.

Discussion

In this manuscript, we report on the development of a dosimetry biomarker management approach to administer precision RAI therapy to patients with mDTC. The ^{124}I PET imaging biomarker provides the treating physician with a tool to select the amount of radioactivity (mCi or MBq) expected to achieve a prescribed radiation-absorbed dose (cGy) to all lesions with SUVs above the selected value likely to achieve a therapeutic response. This manuscript focuses on the biomarker method development, while validation studies with patient outcomes and dose response findings in patients treated in an ongoing study will be discussed in subsequent manuscripts.

Like external beam radiotherapy, it is widely believed that the treatment effectiveness of RAI at the individual lesion level is dependent on the radiation-absorbed dose to the individual lesion. Maxon et al. were among the first to make technically adequate quantitative dose estimates (*14*). These measurements showed complete responses at 8,500 cGy per lesion in 75% of metastatic thyroid cancer lesions to lymph nodes, and a treatment response threshold in a majority of lesions was observed at > 2000 cGy. Based on prior work by Maxon et al., we made an operational definition that a patient with any lesion with a predicted dose of > 2000 cGy would likely respond to treatment (*14*). Therefore, in this study, we used an actionable threshold of 2,000 cGy as the minimum radiation-absorbed dose for the patient to proceed with 131-I RAI therapy, although other thresholds could be used. Consequently, mDTC patients are administered ^{131}I RAI treatment only if they are likely to benefit from it.

Using the proposed approach, we confront a major problem of RAI therapy: the considerable heterogeneity of radiation-absorbed dose to lesions within a given patient, and between patients with mDTC, at a given amount of MBq ^{131}I administered. Variation in measured cGy dose from lesion to lesion may be both technical and biologic in nature. Although the technical features such as difficulty in imaging small tumors quantitatively may play a role in inaccurate dosimetry, it is likely that the observed differences in cGy from lesion to lesion is predominantly biological in nature. This hypothesis is being actively explored.

When investigating single timepoint predictor, the 48-hour timepoint was found to be the best single predictor of the average integrated AUC uptake (directly proportional to cGy dose) for individual lesions. Further research is warranted to explore the impact of characteristics such as clearance, as it can vary greatly from one patient to another, and to encapsulate outlier radioiodine kinetic profiles into the prediction model. This will include extending the regression model to the possibility of adding a second timepoint for the prediction. The current research incorporates useful information about the variability in lesion uptake by considering all lesions from all subjects in the calculation of a prediction interval, in order to best determine the predicted prescribed radioactivity to achieve a radiation-absorbed dose that exceeds the desired threshold for therapeutic efficacy with a stipulated precision, typically 90% or 95% probability. Table 5 provides a useful statistical tool that allows treating clinicians to select a lesion within a patient that they wish to prescribe a radiation dose of at least 2000 cGy. The table columns provide the radioactivity amount that should be administered to have a 50%, 90%, 95%, and 97.5% probability of achieving a 2000 cGy target dose. In patients with multiple lesions, those with higher SUVs at 48h would be expected to receive proportionally higher doses, and those with lower SUVs lower doses. Based on the statistical model derived prediction interval (PI), Table 5 allows physicians to estimate the fraction of a patient's lesion burden that will receive a given radiation dose such as 20000 cGy, which is expected to produce some therapeutic benefit, thereby assisting the physician in determining whether a patient will benefit from radioiodine therapy in all or some of the lesions.

Our approach shows promising results in demonstrating a correlation between integrated AUC and a single timepoint in our learning set of 21 patients, but to further improve the precision of our predictor, recruitment of a larger patient cohort is in process. A simulation study estimated that an increase in sample size from 21 to 60 patients would increase the precision (as measured by the half-width of the 95% PI on the log-scale) from 1.38 to 1.33, but beyond this number, the gain is very small (1.31 and 1.30 with 120 and 1,000 patients, respectively).

Dosimetry for both tumor and normal tissues during RAI and other targeted radiotherapy must be carefully considered if we are to maximize potential benefits for individual patient management. Furthermore, we recognize the unmet need for more optimal dosimetry for both normal

tissues as well as tumors. Other investigators have also recognized this need for a practical single-timepoint imaging method, particularly to assure the patient safety of those undergoing theranostic treatments (*15–29*). Hänscheid et al investigated the accuracy of a single imaging timepoint to predict the dosimetry for key normal tissues and tumor vs. clearance fitting from serial gamma camera images from ^{177}Lu-DOTATATE or ^{177}Lu-DOTATOC treatments (*27*). In that study, they looked at the dose to kidney, liver, spleen, and 30 NET lesions following the administration of ^{177}Lu-DOTATATE or ^{177}Lu-DOTATOC. They studied different timepoints post-administration and found the lowest maximum errors at 96h and reported deviations from the time integral of median of + 5% (range, -9% to + 17%) for kidneys, + 6% (range, -7% to + 12%) for livers, + 8% (range, + 2% to + 20%) for spleens, and + 6% (range, -11% to + 16%) for NET lesions (18). Willowson et al performed a similar study with a focus on kidney dosimetry to anticipate renal toxicity (*17*). They reported an average deviation from doses obtained from complete image data on cycle 1 of 13% and 2% when using 4 h data only and 24 h data only. A recent study by Hou et al (*23*) examined different theranostic agents and suggested that simplified single-timepoint dosimetry approaches may work well for ^{177}Lu-DOTATATE, but the generalizability of single-timepoint imaging for dosimetry for certain targeting agents such as ^{177}Lu-PSMA targeted bone metastases may be less successful.

Finally, personalized radioiodine dosimetry in RAI focused on estimating the MTA would ensure that treatment would not result in a blood and whole-body dose that would exceed the threshold for serious bone suppression or radiation lung fibrosis for patients with extensive lung metastases (10). The shift in dosimetry emphasis being proposed here is toward the rational selection of treatment activity based on a population-averaged statistical model relating single-timepoint ^{124}I lesion SUV measurements with dose expectation and subsequently response prognosis, consistent with the normal tissue-limiting MTA.

Clinically, we recognize that quantitative SPECT imaging is an alternative approach to lesional dosimetry. Since ^{131}I is clinically approved and widely used, potentially developing a single time point approach to lesional dosimetry based on 131I is certainly appealing. However, the ^{124}I PET has major technical advantages mainly related to a combination of higher sensitivity (80–100 times) and better resolution, which translates into significantly better quantitative performance, especially for small metastatic lesions. For these reasons we chose PET and ^{124}I for the proof-of-principal phase of biomarker development and in the setting of clinical research.

In summary, we have provided initial validation of a single time point lesional dosimetry biomarker utilizing 124 I PET scanning. When coupled with a knowledge of the MTA determined by blood and whole-body clearance, clinicians can utilize the relationship between administered activity and lesion al dosimetry to optimize a RAI treatment strategy that maximizes therapeutic effectiveness while minimizing the risk of serious adverse events.

Declarations

Compliance with Ethical Standards

Funding: This study was funded in part by National Cancer Institute (NCI) Cancer Center Support Grant CA008748 and by NCI grant CA201250 (MPIs: Larson/Humm/Ho).

Conflict of Interest: Steven M. Larson, Audrey Mauguen, Alan Ho, Ravinder Grewal, and John Humm are co-inventors of provisional patent for Soothsayer: Number 63/193,700 filed on 5/27/21; conversion deadline: 5/27/22 “Soothsayer”, filed by Office of Technology Development, MSK. SM. Larson reports receiving commercial research grants from Y-mAbs Therapeutics, Inc., Genentech, Inc., WILEX AG, Telix Pharmaceuticals Limited, and Regeneron Pharmaceuticals, Inc.; holding ownership interest/equity in Elucida Oncology, Inc., and holding stock in ImaginAb, Inc., and Y-mAbs Therapeutics. SML is the inventor of issued patents both currently unlicensed and licensed by MSK to Samus Therapeutics, Inc., Elucida Oncology, Inc., and Y-mAbs Therapeutics, Inc. SML serves or has served as a consultant both compensated and uncompensated to Cynvec LLC, Eli Lilly & Co., Prescient Therapeutics Limited, Advanced Innovative Partners, LLC, Gerson Lehrman Group, Progenics Pharmaceuticals, Inc., Exini, Inc., and Janssen Pharmaceuticals, Inc. See https://www.mskcc.org/disclosures?title=Larson%2C%20Steven%20M&company= for further details.

Ethical approval: All procedures performed in studies involving human participants were in accordance with the ethical standards of the institutional and national research committee and with the 1964 Helsinki declaration and its later amendments or comparable ethical standards. All studies were performed under IND #71343, with the prior approval of the MSK Radiation Safety Committee. Compliance issues were fully approved by the Committee on Compliance at MSK.

Informed consent: Informed consent was obtained from all individual participants included in the study.

ACKNOWLEDGMENTS

The authors wish to thank Ryan Min, Senior Research Associate, who skillfully managed all the regulatory and institutional research aspects of the studies performed under IRB #18-253 and #20-253, Leah Bassity for invaluable editorial assistance, the nuclear medicine technologists for performing the imaging, and particularly Pat Zanzonico and his group for providing the blood quantitation.

References

1. Nixon IJ, Whitcher MM, Palmer FL, et al. The impact of distant metastases at presentation on prognosis in patients with differentiated carcinoma of the thyroid gland. *Thyroid.* 2012;22:884–889.
2. Durante C, Haddy N, Baudin E, et al. Long-term outcome of 444 patients with distant metastases from papillary and follicular thyroid carcinoma: benefits and limits of radioiodine therapy. *J Clin Endocrinol Metab.* 2006;91:2892–2899.
3. Pentlow KS, Graham MC, Lambrecht RM, et al. Quantitative imaging of iodine-124 with PET. *J Nucl Med.* 1996;37:1557–1562.
4. Gulec SA, Kuker RA, Goryawala M, et al. (124)I PET/CT in Patients with Differentiated Thyroid Cancer: Clinical and Quantitative Image Analysis. *Thyroid.* 2016;26:441–448.
5. Kist JW, de Keizer B, van der Vlies M, et al. 124I PET/CT to Predict the Outcome of Blind 131I Treatment in Patients with Biochemical Recurrence of Differentiated Thyroid Cancer: Results of a Multicenter Diagnostic Cohort Study (THYROPET). *J Nucl Med.* 2016;57:701–707.
6. Knauf JA, Kuroda H, Basu S, Fagin JA. RET/PTC-induced dedifferentiation of thyroid cells is mediated through Y1062 signaling through SHC-RAS-MAP kinase. *Oncogene.* 2003;22:4406–4412.
7. Ho AL, Grewal RK, Leboeuf R, et al. Selumetinib-enhanced radioiodine uptake in advanced thyroid cancer. *N Engl J Med.* 2013;368:623–632.
8. Dunn LA, Sherman EJ, Baxi SS, et al. Vemurafenib Redifferentiation of BRAF Mutant, RAI-Refractory Thyroid Cancers. *J Clin Endocrinol Metab.* 2019;104:1417–1428.
9. Weber M, Kersting D, Riemann B, et al. Enhancing Radioiodine Incorporation Into Radio Iodine Refractory Thyroid Cancer With MAPK Inhibition (ERRITI): A Single-Center Prospective Two-Arm Study. *Clin Cancer Res.* 2022.
10. Sun F, Gerrard GE, Roberts JK, et al. Ten Year Experience of Radioiodine Dosimetry: is it Useful in the Management of Metastatic Differentiated Thyroid Cancer? *Clin Oncol (R Coll Radiol).* 2017;29:310–315.
11. Benua RS, Cicale NR, Sonenberg M, Rawson RW. The relation of radioiodine dosimetry to results and complications in the treatment of metastatic thyroid cancer. *Am J Roentgenol Radium Ther Nucl Med.* 1962;87:171–182.
12. Furhang EE, Larson SM, Buranapong P, Humm JL. Thyroid cancer dosimetry using clearance fitting. *J Nucl Med.* 1999;40:131–136.
13. Soret M, Bacharach SL, Buvat I. Partial-volume effect in PET tumor imaging. *J Nucl Med.* 2007;48:932–945.
14. Maxon HR, Thomas SR, Hertzberg VS, et al. Relation between effective radiation dose and outcome of radioiodine therapy for thyroid cancer. *N Engl J Med.* 1983;309:937–941.
15. Madsen MT, Menda Y, O'Dorisio TM, O'Dorisio MS. Technical Note: Single time point dose estimate for exponential clearance. *Med Phys.* 2018;45:2318–2324.
16. Del Prete M, Arsenault F, Saighi N, et al. Accuracy and reproducibility of simplified QSPECT dosimetry for personalized (177)Lu-octreotate PRRT. *EJNMMI Phys.* 2018;5:25.
17. Willowson KP, Eslick E, Ryu H, Poon A, Bernard EJ, Bailey DL. Feasibility and accuracy of single time point imaging for renal dosimetry following (177)Lu-DOTATATE ('Lutate') therapy. *EJNMMI Phys.* 2018;5:33.
18. Seo Y, Huh Y, Huang SY, et al. Technical Note: Simplified and practical pretherapy tumor dosimetry - A feasibility study for (131) I-MIBG therapy of neuroblastoma using (124) I-MIBG PET/CT. *Med Phys.* 2019;46:2477–2486.
19. Zhao W, Esquinas PL, Frezza A, Hou X, Beauregard JM, Celler A. Accuracy of kidney dosimetry performed using simplified time activity curve modelling methods: a (177)Lu-DOTATATE patient study. *Phys Med Biol.* 2019;64:175006.
20. Jackson PA, Hofman MS, Hicks RJ, Scalzo M, Violet J. Radiation Dosimetry in (177)Lu-PSMA-617 Therapy Using a Single Posttreatment SPECT/CT Scan: A Novel Methodology to Generate Time- and Tissue-Specific Dose Factors. *J Nucl Med.* 2020;61:1030–1036.
21. Chicheportiche A, Ben-Haim S, Grozinsky-Glasberg S, et al. Dosimetry after peptide receptor radionuclide therapy: impact of reduced number of post-treatment studies on absorbed dose calculation and on patient management. *EJNMMI Phys.* 2020;7:5.
22. Freedman N, Sandström M, Kuten J, et al. Personalized radiation dosimetry for PRRT-how many scans are really required? *EJNMMI Phys.* 2020;7:26.
23. Hou X, Brosch J, Uribe C, et al. Feasibility of Single-Time-Point Dosimetry for Radiopharmaceutical Therapies. *J Nucl Med.* 2021;62:1006–1011.
24. Sandström M, Freedman N, Fröss-Baron K, Kahn T, Sundin A. Kidney dosimetry in 777 patients during (177)Lu-DOTATATE therapy: aspects on extrapolations and measurement time points. *EJNMMI Phys.* 2020;7:73.
25. Devasia TP, Dewaraja YK, Frey KA, Wong KK, Schipper MJ. A Novel Time-Activity Information-Sharing Approach Using Nonlinear Mixed Models for Patient-Specific Dosimetry with Reduced Imaging Time Points: Application in SPECT/CT After (177)Lu-DOTATATE. *J Nucl Med.* 2021;62:1118–1125.
26. Kao YH Single-Time-Point Tumor Dosimetry Assuming Normal Distribution of Tumor Kinetics. *J Nucl Med.* 2022;63:803.

27. Hänscheid H, Lapa C, Buck AK, Lassmann M, Werner RA. Dose Mapping After Endoradiotherapy with (177)Lu-DOTATATE/DOTATOC by a Single Measurement After 4 Days. *J Nucl Med.* 2018;59:75–81.
28. Gustafsson J, Taprogge J. Theoretical aspects on the use of single-time-point dosimetry for radionuclide therapy. *Phys Med Biol.* 2022;67.
29. Sgouros G, Dewaraja YK, Escorcia F, et al. Reply: Single-Time-Point Tumor Dosimetry Assuming Normal Distribution of Tumor Kinetics. *J Nucl Med.* 2022;63:804.

tables

Table 1
Patient demographics

Characteristic	**N = 21***
Age (years)	57 [22–85]
Sex	
Female	8 (38%)
Male	13 (62%)
Stage	
Stage IV	21 (100%)
Thyroglobulin	153 [0–139,750]
Lesions	11 [3–23]
Maximum Tolerated Activity (mCi)	426 [47–896]
Treated	15 (71%)
^{131}**I dose given (mCi)** in treated patients	194 [46–407]

*Median [Range]; n (%)

mCi: milliCurie

Table 2

Abbreviated table of parameters determined for each lesion with measured ^{124}I radioiodine uptake from patient #1

Lesions	Mean size (cm)	Lesion Dose (non-PVC) in cGy	Lesion Dose (PVC) in cGy	T1/2 effective (days)	AUC (uCi.hr)	uCi/g at 48hr	SUV (24hr)	SUV (48hr)	SUV (72hr)	Activity in GBq (mCi) to deliver 2000 cGy	Dose (cGy) from administered 407 mCi treatment	Dose (cGy) at MTA
R. parietal skull	4.03	32.11	41.92	8.02	79.28	0.29	21.9	25.58	25.31	1.77 (47.7)	17063	22345
L. scapula	3.63	20.60	27.73	8.02	50.87	0.20	14.66	17.31	17.55	2.67 (72.1)	11284	14778
R. ant. 2 rib	4.10	16.29	21.18	8.02	40.22	0.15	10.89	13.85	13.18	3.49 (94.4)	8622	11291
L. lateral 7 rib	3.17	18.12	25.72	8.02	44.73	0.17	12.79	14.65	16.07	2.88 (77.8)	10469	13711
L. post elements T3	1.07	2.50	8.89	2.33	6.17	0.05	5.54	3.57	3.52	8.33 (225.0)	3618	4739
spinous process T4	0.77	9.12	51.74	8.02	22.52	0.09	6.56	7.68	8.58	1.43 (38.7)	21056	27575
T7 vertebral body	0.60	7.96	71.05	5.24	19.66	0.10	8.83	8.03	7.68	1.04 (28.1)	28916	37869
L2 vertebral body	0.40	7.14	100.03	4.90	17.63	0.09	7.71	8.26	7.56	0.74 (20.0)	40710	53314
L. post. Acetabulum	4.27	7.88	10.16	6.30	19.46	0.09	7.32	6.87	7.07	7.29 (196.9)	4134	5414
L. post. 5 rib	1.90	1.83	3.59	8.02	4.51	0.02	1.63	1.24	1.25	20.59 (556.4)	1462	1916
L3 vertebral body	0.87	0.71	3.34	2.21	1.76	0.01	1.48	1.35	0.84	22.19 (599.7)	1357	1778
Ant. Aspect of thyroid cartilage	2.00	124.32	234.88	8.02	306.97	1.26	95.8	127.01	84.06	0.31 (8.5)	95597	125193
L. thyroid bed	0.93	7.52	32.00	6.75	18.57	0.08	5.44	7.7	5.31	2.31 (62.5)	13022	17054

cm: centimeters; PVC: Partial volume correction; cGy: centiGray; T1/2: half-life; AUC: Area under the curve; hr: hour; uCi/g: microcurie/gram; mCi: millicurie; R: Right; L: Left; Ant: Anterior; Post: Posterior

Columns 6 and 7 can be converted to MBq.hr and MBq/g by multiplying by 0.037.

Table 3
Prediction of AUC based on the 48h SUV measured, and corresponding activity to be administered to deliver 2000 cGy

SUV at 48h	AUC (uCi.hr/g per mCi)		Activity in GBq (mCi) to deliver 2000 cGy				
	Mean Estimate	95% PI	To target 50% of the lesions - Mean Estimate	To target 90% of the lesions (90% upper bound)	To target 95% of the lesions (95% upper bound)	To target 97.5% of the lesions (Upper bound of the 95% PI)	Lower bound of the 95% PI
2	4.0	1.5–9.1	45.4 (1228.1)	2236.5	2612.8	3200.4	542.4
4	8.1	3.3–20.3	22.7 (613.2)	1066.4	1278.0	1474.6	243.5
6	12.1	4.8–29.2	15.1 (408.5)	759.4	890.6	1032.0	168.9
8	16.1	6.4–38.8	11.3 (306.2)	570.5	692.4	775.6	127.4
10	20.2	8.6–48.4	9.06 (244.8)	431.4	517.0	576.6	102.1
15	30.3	11.9–71.0	6.03 (163.1)	292.3	355.5	416.2	69.6
20	40.4	16.1–97.1	4.52 (122.2)	217.6	254.8	306.9	50.9
30	60.6	24.3–147.4	3.01 (81.4)	153.1	179.1	202.9	33.5
50	101.2	40.8–252.9	1.81 (48.8)	87.9	102.7	121.1	19.5
100	202.6	82.3–479.6	0.90 (24.4)	45.3	53.1	60.0	10.3
200	405.8	164.2–951.2	0.45 (12.2)	21.5	26.0	30.1	5.2
300	609.2	257.8–1476.2	0.30 (8.1)	14.5	16.7	19.2	3.3

SUV: Standardized uptake value; AUC: Area under the curve; uCI: microCurie; hr: hour; g: gram; mCi: millicurie; cGy: centiGray; PI: Prediction interval

Column 2 is in units of MBq.hr/g per GBq or uCi.hr/g per mCi.

Column 4 is in units of GBq with the equivalent mCi amounts provided in brackets.

Table 4
Estimate of linear regression parameters, prediction error, and cross-validated prediction error, and estimated required activity to deliver 2,000 cGy for different predictors using one timepoint

Timepoint	N	Slope	Robust se	Squared Error	CV Squared Error
uCi 24hr	231	1.018	0.050	0.615	0.665
uCi 48hr	231	0.934	0.043	0.443	0.484
uCi 72hr	231	0.859	0.051	0.679	0.761
SUV 24hr	217	1.057	0.045	0.436	0.472
SUV 48hr	**208**	**1.002**	**0.024**	**0.204**	**0.223**
SUV 72hr	193	0.963	0.039	0.292	0.327
SUL 24hr	211	1.062	0.046	0.403	0.434
SUL 48hr	**200**	**1.013**	**0.028**	**0.207**	**0.225**
SUL 72hr	186	0.955	0.044	0.301	0.338
uCi: microCurie; hr: hour; se = standard-error; CV: cross-validated; cGy: centiGray.					

Figures

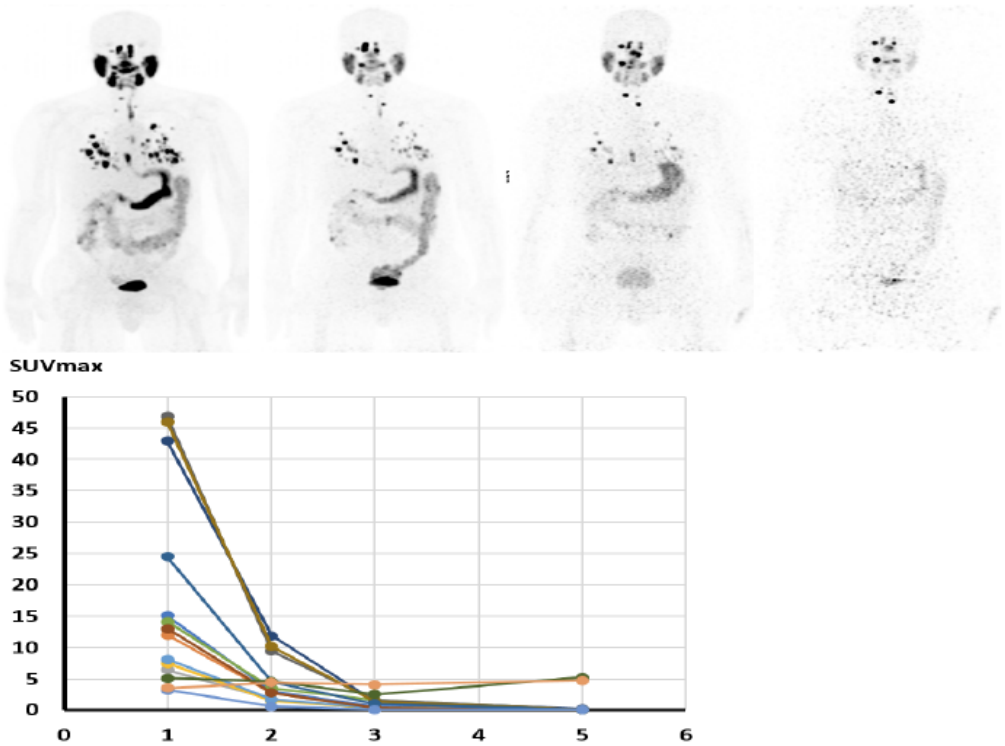

Figure 1

Example of four ^{124}I PET scans conducted at 24, 48, 72, and 120 hours post-oral radioiodine administration. The clearance curves (SUVmax plotted vs. time in days) for individual neck and lung lesions of size >0.5cc) is shown in the view graph. This patient demonstrates a case with lung lesions exhibiting high radioiodine uptake and rapid clearance alongside neck nodes with low uptake but slow clearance

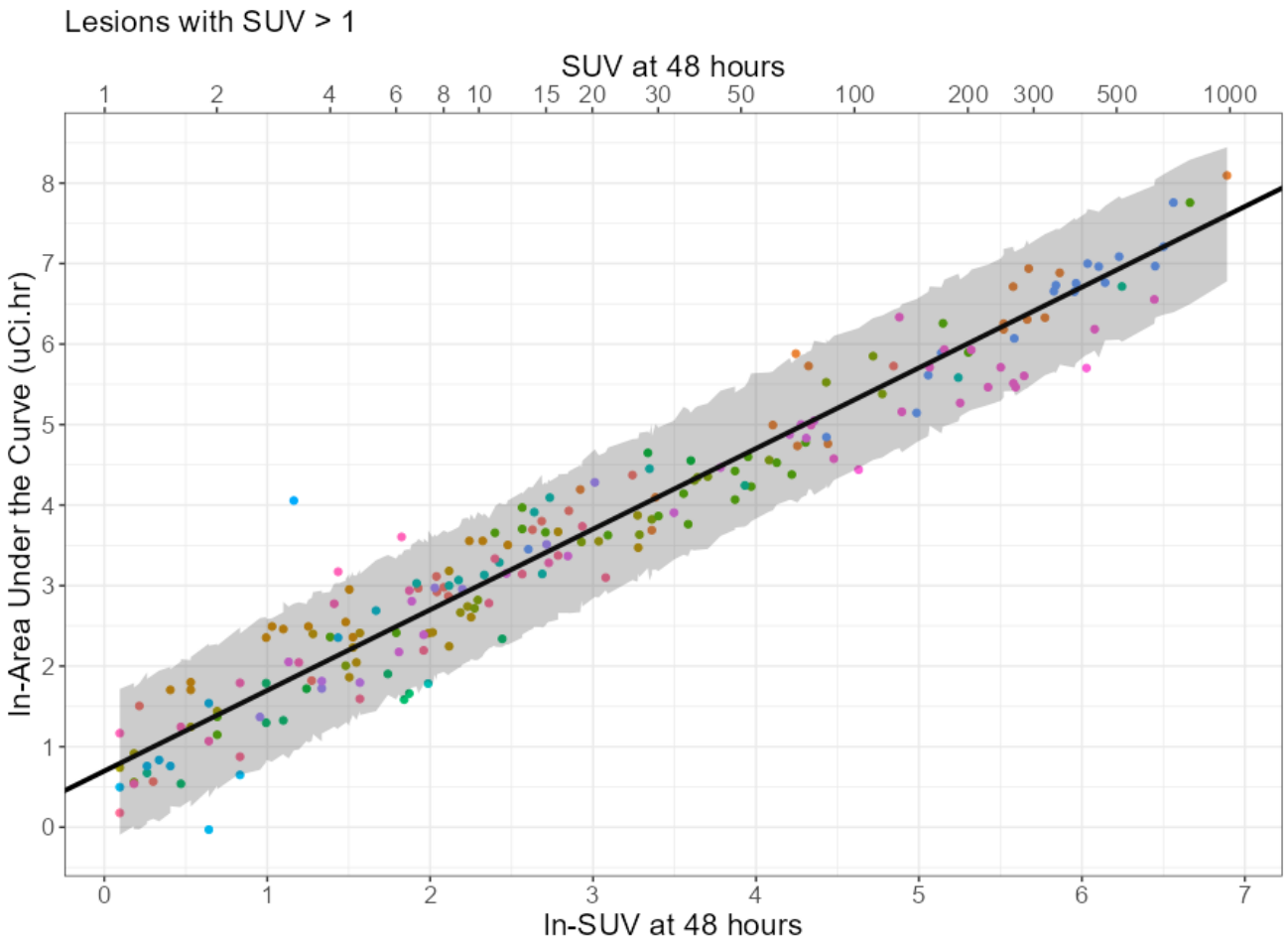

Figure 2

Prediction curve for the best predictor as the ^{124}I PET imaging biomarker. 48h SUV (optimal predictor) vs. AUC (each color represents a patient; each dot is a lesion; black line is the average linear regression line from the GEE estimate while gray area is the 95% prediction interval)

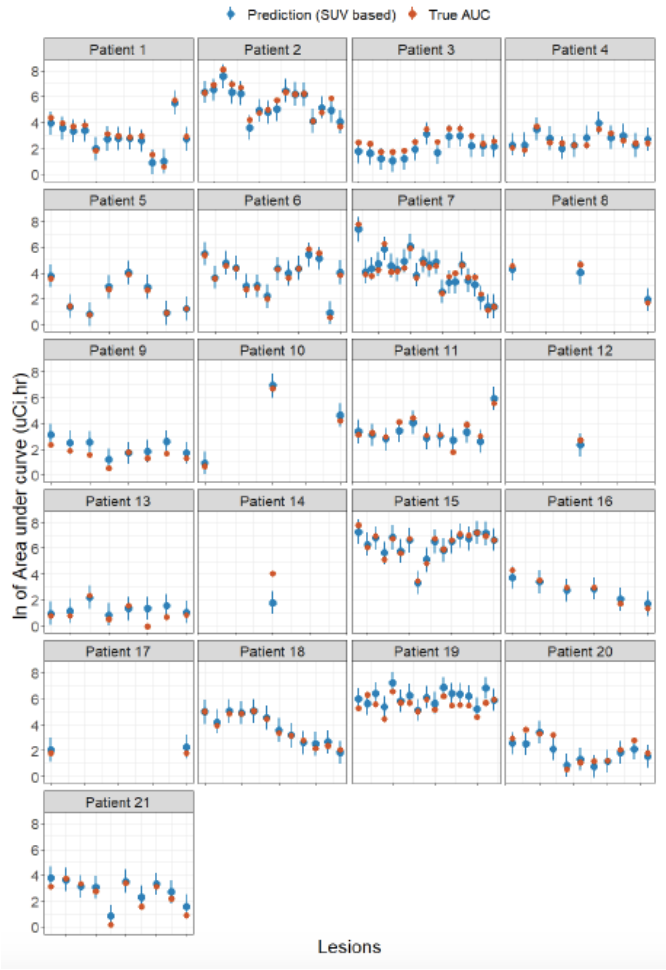

Figure 3

Results of leave-one-out cross-validation (SUV analysis). For each patient (separate quadrant), the AUC as predicted by our model is represented by a blue point while the blue line represents the 95% PI. The orange dots represent the actual AUC as measured on the lesion

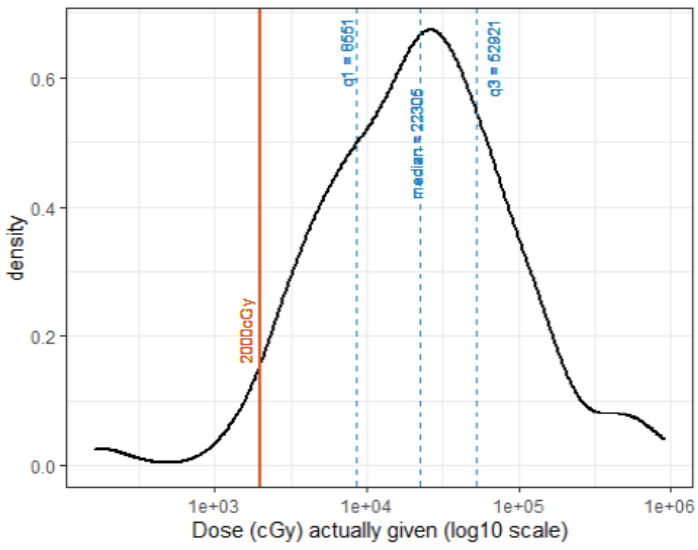

Figure 4

Distribution of radioactive iodine treatment dose given in 169 treated lesions (15 patients)

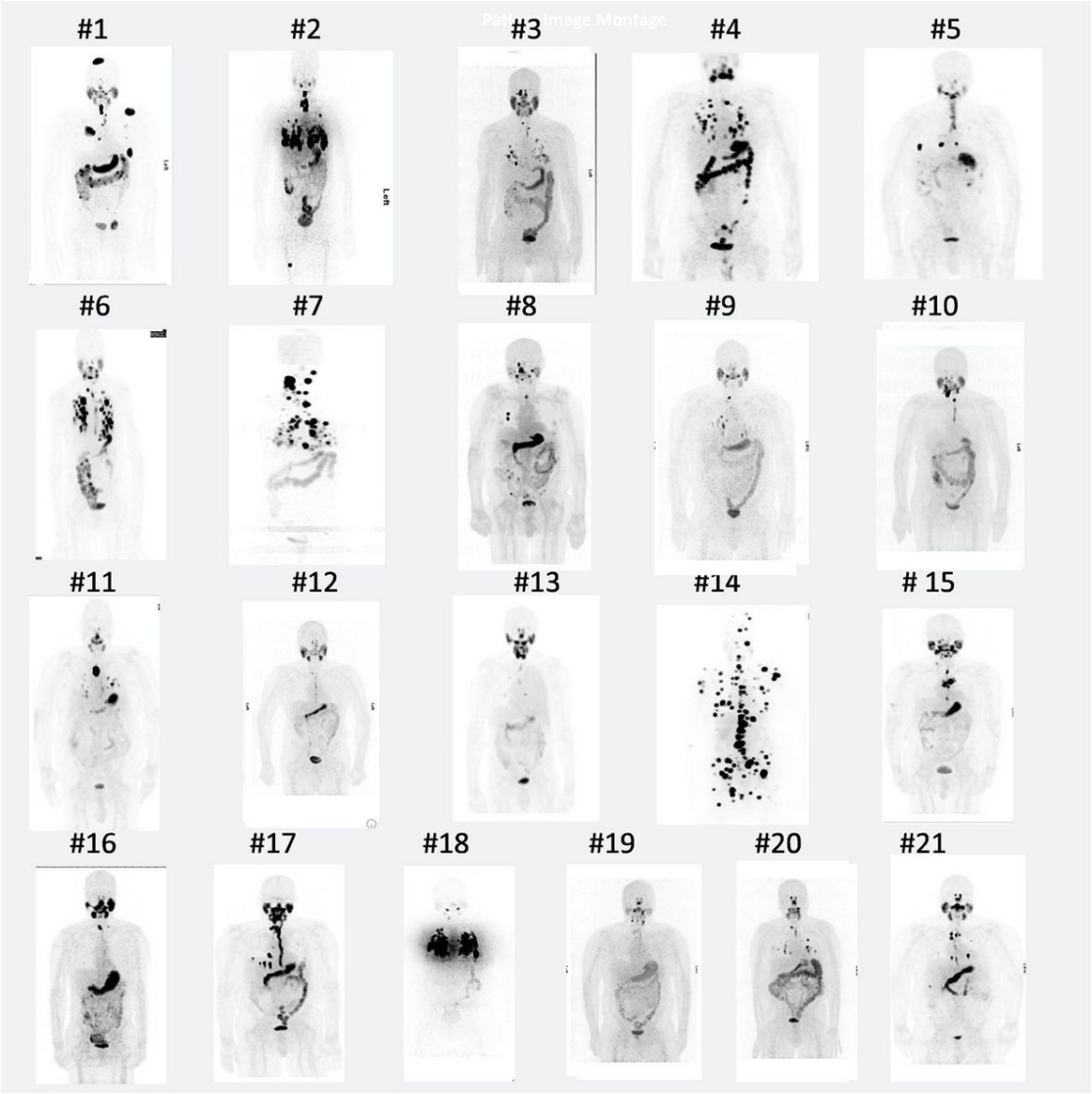

Figure 5

Maximum intensity projection (MIP) PET ^{124}I images at 48 hours of 21 patents in teaching set

Supplementary Files

This is a list of supplementary files associated with this preprint. Click to download.

- SoothsayermanuscriptAppendix.docx
- SupplementalTable1.docx